NUMERICAL STUDY ON NATURAL CONVECTION IN THREE -DIMENSIONAL RECTANGULAR ENCLOSURES

Taik Sik Lee*, Gi Hun Son* and Joon Sik Lee*

(Received March 18, 1989)

Natural convection in three-dimensional rectangular enclosures has been analyzed numerically using a strongly stabilized QUICK(Quadratic Upstream Interpolation for Convective Kinematics) scheme. Computations are performed for the different cases of temperature boundary conditions to see the effect of temperature disturbance on three-dimensional motion. The effect of the Rayleigh number is mainly investigated and two dimensional approximation limit is examined as well. The results show that the temperature disturbance imposed on the end wall reinforces the axial flow and magnifies the three-dimensional effect.

Key Words: QUICK Scheme, Temperature Disturbance, Secondary Flow

NOMENCLATURE

A_Y : Y-directional aspect ratio
A_Z : Z-directional aspect ratio
c : Specific heat
g : Gravitational acceleration
k : Thermal conductivity
L : Length of the box in the X direction
Nu_l : Local Nusselt number
Nu_m : Mean Nusselt number
P : Pressure
Pr : Prandtl number
T : Temperature
T_h : Temperature of the hot wall
T_c : Temperature of the cold wall
T_0 : Reference temperature
Q_X : Volume flow rate in the X direction
Q_Y : Volume flow rate in the Y direction
Ra : Rayleigh number
U, V, W : Velocity components
V : Velocity vector
X, Y, Z : Coordinates
α : Thermal diffusivity
Γ : Diffusion coefficient
θ : Dimensionless temperature
ρ : Fluid density
ϕ : General dependent variable

Subscripts

E, EE, P, W, WW : Grid points(Fig. 2)
b, e, m, n, s, t, w : Control surface(Fig. 2)

1. INTRODUCTION

For many years a lot of attention has been paid to the problems of natural convection in enclosures. However, the limitations of mathematical tools and experimental techniques restrict investigators within the approximation of a two-dimensional model even though fluid motion is three-dimensional in nature. Recently, the development of numerical methods for the solutions of the three-dimensional flow with high accuracy and strong stability extricates the explorers from the hurdle of the two-dimensional limitation.

Mallinson and de Vahl Davis(1977) investigated three-dimensional effects induced by velocity disturbance due to the existence of the end walls. They show that the three-dimensional motion is due to the interaction of the rotating flow with the stationary walls together with a contribution arising from buoyancy forces generated by longitudinal temperature gradients. Morrison and Tran(1977) conducted experimental study on the flow structure generated by heat transfer in a vertical rectangular cavity with aspect ratio of 5. The measurements show that the end wall conduction affects the whole flow structure and thus may introduce significant deviations from the commonly assumed two-dimensional conditions in the central section. Mallinson(1987) investigated numerically the three-dimensional effects using the Hele Shaw model. The results for side heating and heating from below overpredict the heat transfer.

In this study, three different cases described below, have been considered to account for the three-dimensional effect due to a temperature disturbance.

[Case I] the right wall is at a higher temperature than that of the left wall, all other walls being adiabatic

[Case II] the right wall is at a higher temperature than that of the left wall and the front and rear walls have a linear temperature profile in the horizontal direction, the top and bottom walls being adiabatic

[Case III] the front and rear walls have a linear temperature distribution in the horizontal direction, all other walls being adiabatic.

The orientations of the walls are given in Fig. 1.

QUICK scheme is employed in the calculation and to improve the convergence of this scheme, some terms appearing in the finite difference equation are rearranged in a manner to obey Patankar's rule(1980).

Calculations are performed for the three different Rayleigh

*Department of Mechanical Engineering, Seoul National University, Seoul 151-742, Korea

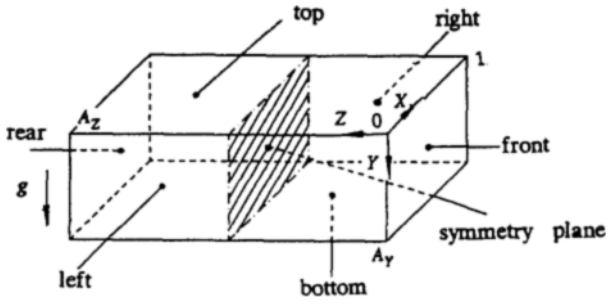

Fig. 1 Configuration and coordinate system

numbers of 10^4, 10^5 and 10^6 and in each case the streamline, velocity profile and Nusselt number variation are presented.

2. ANALYSIS

2.1 Mathematical Model

The configuration and coordinate system of the problem is shown in Fig. 1, the length being nondimensionalized by L, the size of the box in the X-direction. By introducing scale factors, α/L and $\rho\alpha^2/L^2$, for velocity and pressure respectively, and defining dimensionless temperature, $\theta=(T-T_0)/(T_h-T_c)$, where T_0 is the initial temperature of the fluid in the enclosure, it follows that the governing equations for steady Boussinesq convection become

$$\nabla\cdot V=0, \tag{1}$$

$$\nabla\cdot(VV)=-\nabla P+Pr\nabla^2 V+RaPr\theta g, \tag{2}$$

$$\nabla\cdot(V\theta)=\nabla^2\theta, \tag{3}$$

where Ra and Pr are Rayleigh and Prandtl numbers respectively.

The velocity boundary conditions at the walls are given as $V=0$. For temperature, $\nabla\theta\cdot n=0$ at the horizontal walls for all cases, but those of other walls are different in the three cases. With the assumption of symmetry about the $Z=A_Z/2$ plane, the calculation domain can be confined to the half of the box, and the boundary conditions tabulated in Table 1 can be applied.

2.2 Numerical Method

Introducing the general variable ϕ and the diffusion coefficient Γ, the governing equation in a steady one-dimensional problem is

$$\frac{\partial}{\partial X}\left(\rho U\phi-\Gamma\frac{\partial\phi}{\partial X}\right)=0. \tag{4}$$

Integration of Eq. (4) over the uniform control volume shown in Fig. 2 yields

$$\left(\rho U\phi-\Gamma\frac{\partial\phi}{\partial X}\right)_e-\left(\rho U\phi-\Gamma\frac{\partial\phi}{\partial X}\right)_w=0. \tag{5}$$

Leonard(1979) suggested the following quadratic upstream interpolation of convective variables to remove false diffusion problem of upwind scheme.

$$U_e>0:\ \phi_e=\phi_P+\left(\frac{\partial\phi}{\partial X}\right)_P\frac{\delta x}{2}+\left(\frac{\partial^2\phi}{\partial X^2}\right)_P\frac{\delta x^2}{8}, \tag{6}$$

Table 1 Temperature boundary conditions for each case

	Case I	Case II	Case III
Front wall	Adiabatic	$\theta=X-0.5$	$\theta=X-0.5$
Left wall	$\theta=-0.5$	$\theta=-0.5$	Adiabatic
Right wall	$\theta=0.5$	$\theta=0.5$	Adiabatic

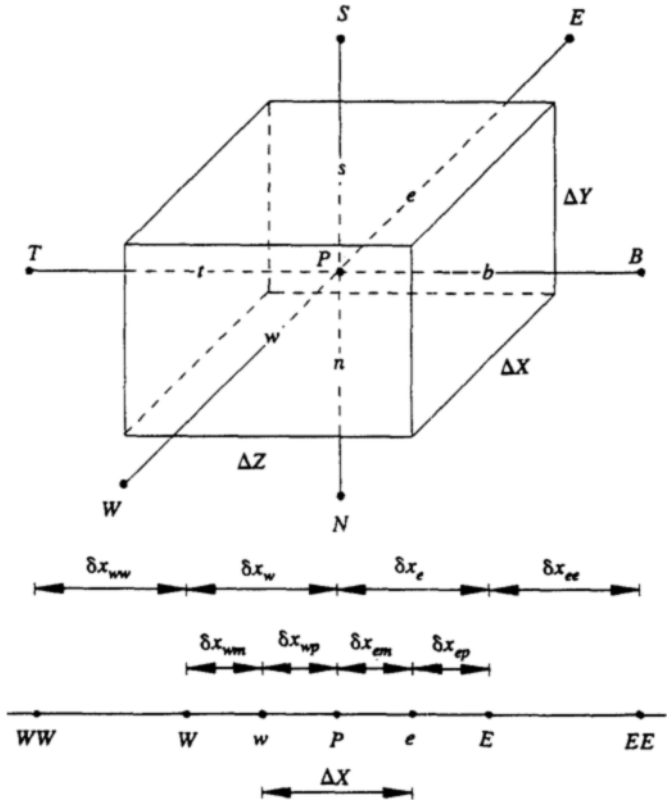

Fig. 2 Control volume

$$U_e<0:\ \phi_e=\phi_E-\left(\frac{\partial\phi}{\partial X}\right)_E\frac{\delta x}{2}+\left(\frac{\partial^2\phi}{\partial X^2}\right)_E\frac{\delta x^2}{8}, \tag{7}$$

and

$$\left(\frac{\partial\phi}{\partial X}\right)_e=\frac{\phi_E-\phi_P}{\delta x}, \tag{8}$$

where

$$\left(\frac{\partial\phi}{\partial X}\right)_P=\frac{\phi_P-\phi_W}{2\delta x}-\frac{\phi_P-\phi_E}{2\delta x}, \tag{9}$$

$$\left(\frac{\partial^2\phi}{\partial X^2}\right)_P=-\frac{\phi_P-\phi_W}{\delta x^2}-\frac{\phi_P-\phi_E}{\delta x^2}. \tag{10}$$

However, it has been found that the direct application of Leonard's QUICK scheme involves convergence problem especially for the high Peclet numbers. Therefore, in this study, the terms appearing in finite difference equation are rearranged to meet Patankar's rule.

By integration of Eq. (4) over the control volume ($X_w<X<X_e$, $Y_s<Y<Y_n$, $Z_b<Z<Z_t$), the following equation may be obtained.

$$\int_{Z_b}^{Z_t}\int_{Y_s}^{Y_n}\left\{\left(\rho U\phi-\Gamma\frac{\partial\phi}{\partial X}\right)_e-\left(\rho U\phi-\Gamma\frac{\partial\phi}{\partial X}\right)_w\right\}dYdZ$$
$$=A_E(\phi_P-\phi_E)+A_W(\phi_P-\phi_W)-B_E$$
$$=A_{E_1}(\phi_P-\phi_E)+A_{W_1}(\phi_P-\phi_W)-B_{E_1}$$
$$+A_{E_2}(\phi_P-\phi_E)+A_{W_2}(\phi_P-\phi_W)-B_{E_2}, \quad (11)$$

where A_E, A_W, and B_E are as follows.

$A_E=A_{E_1}+A_{E_2}$, $A_W=A_{W_1}+A_{W_2}$, $B_E=B_{E_1}+B_{E_2}$.

Each term in the integrand in Eq. (11) may be expressed separately as

$$\int_{Z_b}^{Z_t}\int_{Y_s}^{Y_n}\left(\rho U\phi-\Gamma\frac{\partial\phi}{\partial X}\right)_e dYdZ$$
$$=A_{E_1}(\phi_P-\phi_E)+A_{W_1}(\phi_P-\phi_W)-B_{E_1}, \quad (12)$$
$$\int_{Z_b}^{Z_t}\int_{Y_s}^{Y_n}\left(\rho U\phi-\Gamma\frac{\partial\phi}{\partial X}\right)_w dYdZ$$
$$=A_{E_2}(\phi_P-\phi_E)+A_{W_2}(\phi_P-\phi_W)-B_{E_2}. \quad (13)$$

Defining $F_e=(\rho U)_e\Delta Y\Delta Z$, and $D_e=\frac{\Gamma_e}{\delta x_e}\Delta Y\Delta Z$, and introducing QUICK scheme to Eq. (12) yields

$$\int_{Z_b}^{Z_t}\int_{Y_s}^{Y_n}\left(\rho U\phi-\Gamma\frac{\partial\phi}{\partial X}\right)_e dYdZ$$
$$=[F_e,\ 0]\{\phi_P+(\phi_P-\phi_W)(C_1-C_3)$$
$$+(\phi_P-\phi_E)(-C_2-C_4)\}$$
$$+[-F_e,\ 0]\{-\phi_E+(\phi_P-\phi_E)(-C_9-C_{11})$$
$$+(\phi_E-\phi_{EE})(-C_{10}+C_{12})\}+D_e(\phi_P-\phi_E)$$
$$=[-F_e,\ 0](1-C_9-C_{11})(\phi_P-\phi_E)$$
$$+[F_e,\ 0](C_1-C_3)(\phi_P-\phi_W)$$
$$+[F_e,\ 0]\{\phi_P-(C_2+C_4)(\phi_P-\phi_E)\}$$
$$+[-F_e,\ 0]\{-\phi_P+(-C_{10}+C_{12})(\phi_E-\phi_{EE})\}$$
$$=A_{E_1}(\phi_P-\phi_E)+A_{W_1}(\phi_P-\phi_W)+B_{E_1}. \quad (14)$$

Now the coefficients A_{E_1} and A_{W_1} are rearranged to have positive values as follows:

$$A_{E_1}=[-F_e,\ 0](1-C_9-C_{11})+D_e,$$
$$A_{W_1}=[F_e,\ 0](C_1-C_3),$$
$$B_{E_1}=[F_e,\ 0]\{\phi_P-(C_2+C_4)(\phi_P-\phi_E)\}$$
$$-[-F_e,\ 0]\{\phi_P+(C_{10}-C_{12})(\phi_E-\phi_{EE})\}, \quad (15)$$

where the coefficients C's are:

$$C_1=\frac{\delta x_e\delta x_{em}}{\delta x_w(\delta x_w+\delta x_e)},\quad C_2=\frac{\delta x_w\delta x_{em}}{\delta x_e(\delta x_w+\delta x_e)},$$
$$C_3=\frac{\delta x_{em}^2}{\delta x_w(\delta x_w+\delta x_e)},\quad C_4=\frac{\delta x_{em}^2}{\delta x_e(\delta x_w+\delta x_e)},$$
$$C_9=\frac{\delta x_{ee}\delta x_{ep}}{\delta x_e(\delta x_e+\delta x_{ee})},\quad C_{10}=\frac{\delta x_e+\delta x_{ep}}{\delta x_{ee}(\delta x_e+\delta x_{ee})},$$
$$C_{11}=\frac{\delta x_{ep}^2}{\delta x_e(\delta x_e+\delta x_{ee})},\quad C_{12}=\frac{\delta x_{ep}^2}{\delta x_{ee}(\delta x_e+\delta x_{ee})}.$$

Similary following equations are obtained corresponding to Eq. (13).

$$A_{E_2}=[-F_e,\ 0](D_{10}-D_{12}),$$
$$A_{W_2}=[F_w,\ 0](1-D_2-D_4)+D_w, \quad (16)$$
$$B_{E_2}=[-F_w,\ 0]\{\phi_P-(D_9+D_{11})(\phi_P-\phi_W)$$
$$+[F_e,\ 0]\{-\phi_P-(D_1-D_3)(\phi_W-\phi_{WW})\},$$

where the coefficients D's are:

$$D_1=\frac{\delta x_w\delta x_{wm}}{\delta x_{ww}(\delta x_{ww}+\delta x_w)},\quad D_2=\frac{\delta x_{ww}\delta x_{wm}}{\delta x_w(\delta x_{ww}+\delta x_w)},$$
$$D_3=\frac{\delta x_{wm}^2}{\delta x_{ww}(\delta x_{ww}+\delta x_w)},\quad D_4=\frac{\delta x_{wm}^2}{\delta x_w(\delta x_{ww}+\delta x_w)},$$
$$D_9=\frac{\delta x_e\delta x_{wp}}{\delta x_w(\delta x_w+\delta x_e)},\quad D_{10}=\frac{\delta x_w\delta x_{wp}}{\delta x_e(\delta x_w+\delta x_e)},$$
$$D_{11}=\frac{\delta x_{wp}^2}{\delta x_w(\delta x_w+\delta x_e)},\quad D_{12}=\frac{\delta x_{wp}^2}{\delta x_e(\delta x_w+\delta x_e)}.$$

At the boundary the modified gradient with second order accuracy is employed in the form of

$$\left(\frac{\partial\phi}{\partial X}\right)_0=\frac{\phi_P-\phi_W}{2\delta x}+\frac{3\phi_P-2\phi_W-\phi_{EE}}{3\delta x}. \quad (17)$$

A staggered grid system is adopted for the velocity components and SIMPLE algorithm is employed for the correction of pressure field to satisfy the continuity.

3. RESULTS AND DISCUSSION

The present discussion starts by considering the results corresponding to the box with $A_X=1$, $A_Y=1$ and $A_Z=2$, with $Pr=0.71$ and with the Rayleigh numbers of 10^4, 10^5 and 10^6. Then, the case, $A_z=4$ is included to investigate the conditions for the two-dimensional approximation by means of the penetration depth of the three-dimensional effect.

Solutions are obtained with $22\times22\times22$ mesh which is

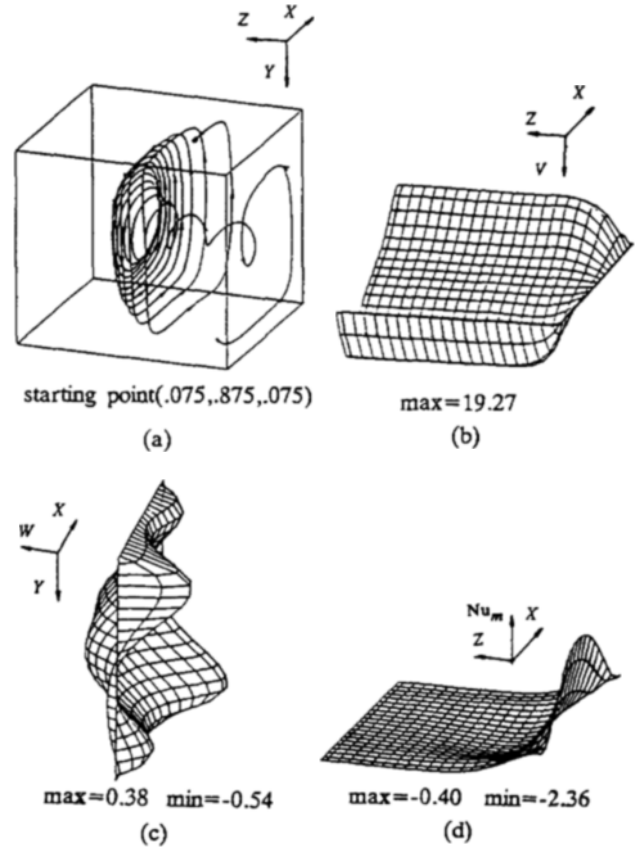

Fig. 3 Streamline, velocity, and mean Nusselt number distribution in Case I for $Ra=10^4$ and $A_Z=2$, (a) streamline, (b) V velocity on $X-Z$ plane at $Y=0.5$, (c) W velocity on $X-Y$ plane at $Z=0.05$, (d) mean Nusselt number distribution on $X-Z$ plane

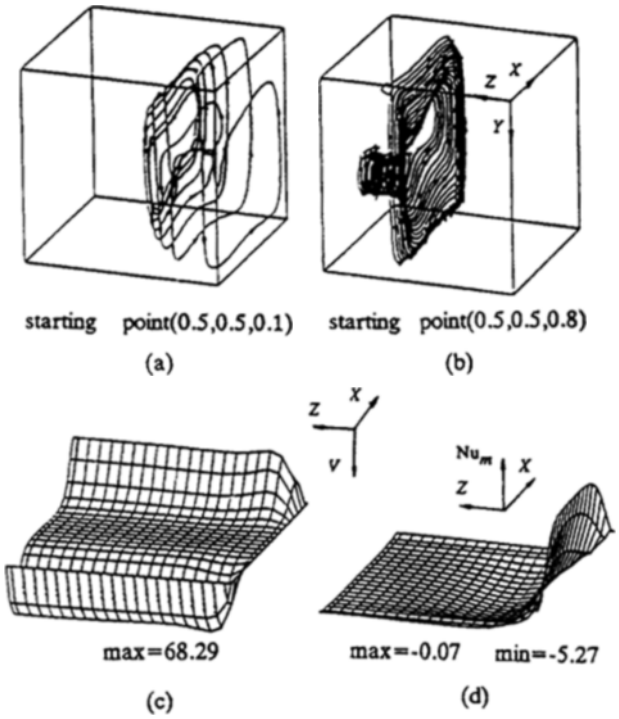

Fig. 4 Streamline, velocity, and mean Nusselt number distribution in Case I for $Ra=10^5$ and $A_z=2$, (a), (b) streamline, (c) V velocity on $X-Z$ plane, (d) mean Nusselt number distribution on $X-Z$ plane

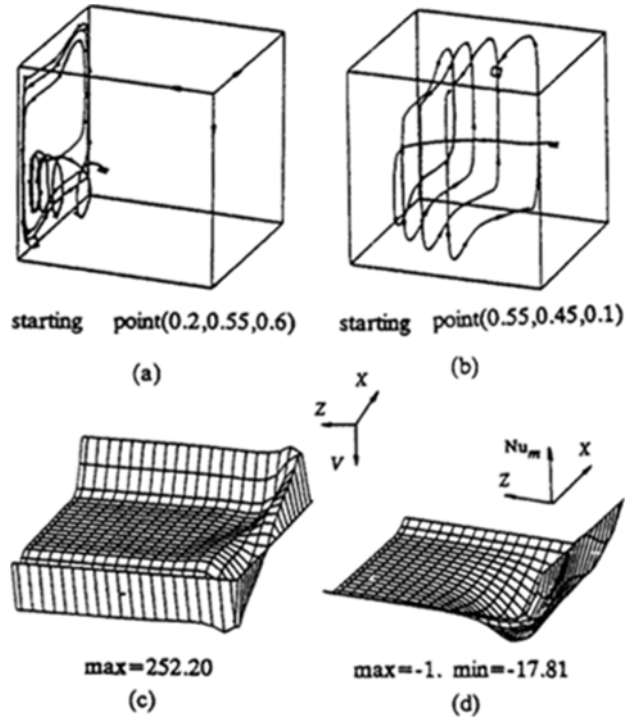

Fig. 5 Streamline, velocity, and mean Nusselt number distribution in Case I for $Ra=10^6$ and $A_z=2$, (a), (b) streamline, (c) V velocity on $X-Z$ plane at $Y=0.5$, (d) mean Nusselt number distribution on $X-Z$ plane

considered to give reasonable compromise between accuracy and computing cost.

In the figures, to draw a streamline, the velocity components at a prescribed starting point are found by interpolation from the values at the surrounding mesh points and increments in the particle position are obtained by integration using a fourth-order Runge-Kutta method. The mean Nusselt number, Nu_m, is obtained by averaging the local Nusselt number over the length in the Y-direction. The local Nusselt number at a point in the box is defined as

$$Nu_l=\frac{\rho cUT-k\dfrac{\partial T}{\partial X}}{(k/L)(T_h-T_c)}. \tag{18}$$

[Case I]

Figures. 3, 4 and 5 show the streamlines, velocities and mean Nusselt number distributions for the Rayleigh numbers of 10^4, 10^5 and 10^6 respectively.

The interaction of a rotating roll with an end wall (front or rear wall) is often explained by a model of a rotating cylinder with a stationary end wall. The axial flow is directed away from the end wall and returned outward to the end wall as shown in Fig. 3(a). In this case, the rotational motion is driven by the buoyancy force due to the temperature difference between side walls instead of by the shearing with the rotating wall of the cylinder. The spiral streamline pattern shown in Fig. 3(a) is a consequence of the superposition of the axial flow induced to satisfy the continuity on the crosssectional flow due to buoyancy. A relatively strong axial flow near the end wall is getting absorbed into the crosssectional flow as it moves into the depth and returns to within a small distance from the starting point to form a closed streamline. This three-dimensional flow can be produced by two mechanisms. The first is the kinematic interaction of the rotating fluid with the stationary plane and the second is thermal interaction resulting from axial temperature gradient. Detailed discussion may be found elsewhere(Mallinson et al., 1977).

For the high Rayleigh numbers($Ra=10^5$, 10^6), the secondary rolls appear due to the convective distortion of the temperature field. As the Rayleigh number increases, the thermal boundary layer is getting thinner and hence the temperature gradient in the vicinity of the wall is intensified to retain the viscous diffusion. This secondary flow induces the flow in the negative Z direction along the axis of this secondary flow. This flow is separated from the one in the positive Z direction, which arises to make balance the centrifugal and pressure forces near the end wall(Fig. 4(a) and 4(b)).

However, the end wall effect is confined to the vicinity of the wall. Due to the nonlinear increase in the strength of the crosssectional flow or maximum of V velocity as indicated in Fig. 3(b), 4(c) and 5(c), the viscous diffusion does not smear far into the central region and is confined to this thin layer.

The mean Nusselt number variation may give a criterion whether the flow can be approximated as two dimensional, since this distribution should be uniform on $X-Z$ plane in the case of two dimensional flow. It can be seen by the comparison of Fig. 3(d), 4(d) and 5(d), the end effect is confined to the vicinity of the end wall as the Rayleigh number increases.

[Case II]

The aim of the present case is to predict the effect of the temperature disturbance imposed on the end wall. This disturbance may arise from conduction between the hot and cold side walls through the end wall. The profile may not be

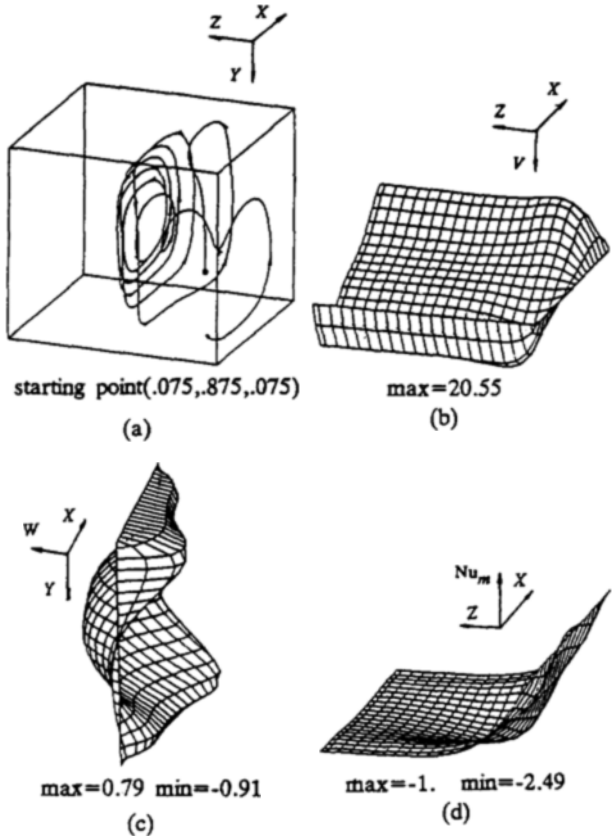

Fig. 6 Streamline, velocity, and mean Nusselt number distribution in Case II for $Ra=10^4$ and $A_z=2$, (a) streamline, (b) V velocity on $X-Z$ plane at $Y=0.5$, (c) W velocity on $X-Y$ plane at $Z=0.05$, (d) mean Nusselt number distribution on $X-Z$ plane

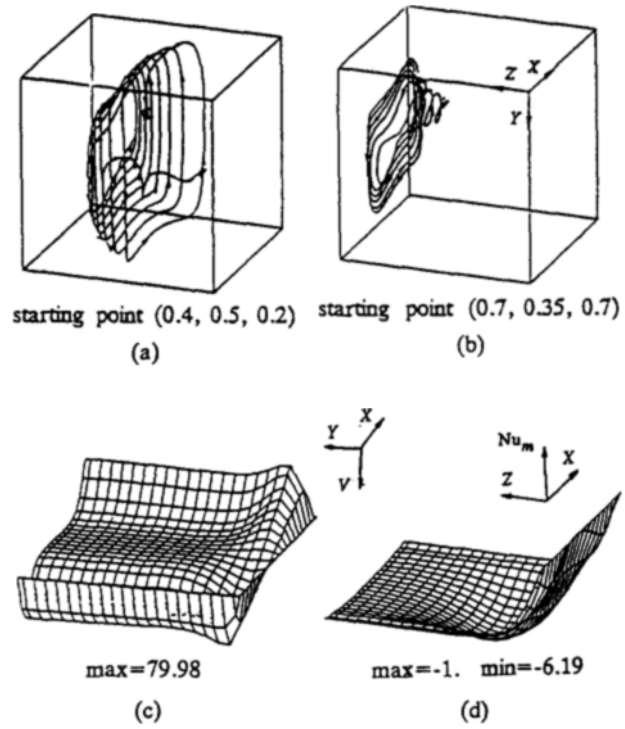

Fig. 7 Streamline, velocity and mean Nusselt number distribution in Case II for $Ra=10^5$ and $A_z=2$, (a), (b) streamline, (c) V velocity on $X-Z$ plane at $Y=0.5$, (d) mean Nusselt number distribution on $X-Z$ plane

exactly linear due to the convection from or to the end wall, however, it can be reasonably assumed to be linear.

Figures. 6, 7 and 8 show the representative results according to the Rayleigh numbers.

From fluid dynamics point of view, this flow may be modeled as the one in a rotating cylinder with a rotating end wall. In the case of no temperature disturbance, the axial velocity throughout the roll must be small due to the relatively small rates of rotation. When the temperature disturbance is introduced, large rotational flow is induced in the vicinity of the end wall and it reinforces the axial flow.

In the case of steady flow, streamlines are identical to particle trajectories. In Fig. 6(a), the fluid particle started at (.075, .875, .075) is pushed away from the end wall in the initial rolling motion and it sustains axial directional motion. The rotational motion is quite reduced in this case compared to the particle motion shown in Fig. 3(a). V velocity distribution plotted in Fig. 6(b) shows that the viscous diffusion penetrates somewhat deeply into the core region at $Ra=10^4$.

The skewed W velocity profile shown in Fig. 6(c) illustrates the effect of the temperature disturbance. Due to the upward flow near the right half of the front wall, where the wall is hotter than the fluid, W velocity in the negative Z direction is retarded, and it is reversed near the left half.

At $Ra=10^5$, the fluid particle started near the center of $X-Y$ plane experiences several rotational motion before it returns (Fig. 7(a)), however, at $Ra=10^6$, the fluid particle

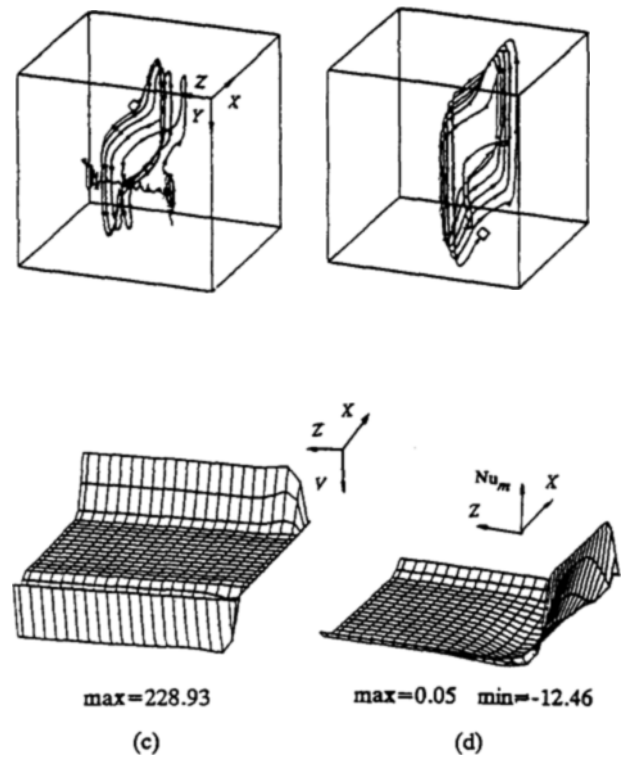

Fig. 8 Streamline, velocity and mean Nusselt number distribution in Case II for $Ra=10^6$ and $A_z=2$, (a), (b) streamline, (c) V velocity on $X-Z$ plane at $Y=0.5$, (d) mean Nusselt number distribution on $X-Z$ plane

directly moves deeply towards the plane of symmetry without rotational motion. Since the boundary layer is much thinner at $Ra=10^6$ than that at $Ra=10^5$ as shown in V velocity distributions plotted in Fig. 7(c) and 8(c), the primary rotational motion is circumscribed in the thin layer and the fluid particle passing through the very core region is not affected. Fig. 8(a) shows the formation of the secondary roll which is frequently seen in two-dimensional plots at the high Rayleigh numbers. The linear temperature disturbance is expected to act favorable for the two dimensionality since it induces a large rotational flow near the end wall as shown in Fig. 6(a). However, the mean Nusselt number distributions compared with those of Case I show that the three dimensional effect penetrates more into the Z direction.

〔**Case** III〕

Case III is employed to investigate the sole effect of the temperature disturbance on the three dimensionality and the length of the box in the Z direction is elongated twice as long as before to allow enough penetration depth for the three dimensional effect. Volume flow rates, Q_X and Q_Y, in a plane perpendicular to the Z axis is made of parameters to measure the penetration depth of the three dimensional effect, since these values should remain constant in the case of two dimensional flow. Q_X and Q_Y are defined as

$$Q_X=\int_0^{AY/2} UdY \quad \text{at} \quad X=0.5, \tag{19}$$

$$Q_Y=\int_0^{0.5} VdX \quad \text{at} \quad Y=\frac{A_Y}{2}. \tag{20}$$

Figure 9 shows Q_X and Q_Y variations along the Z axis. As shown in the figure, the three dimensional effect penetrates more deeply in Case II than in Case I. Now the reason is obvious from the sole effect of temperature disturbance (Case III) which shows strong three-dimensional behavior. For $Ra=10^4$, the three dimensionality of U velocity (or Q_X) and V velocity (or Q_Y) is almost the same, but for the high Rayleigh numbers, the three dimensionality of U velocity is much stronger than that of V velocity. This is due to the rapid pumping of fluid along the Y direction in the thin boundary layer on the side walls, which dispels the effect of the end wall.

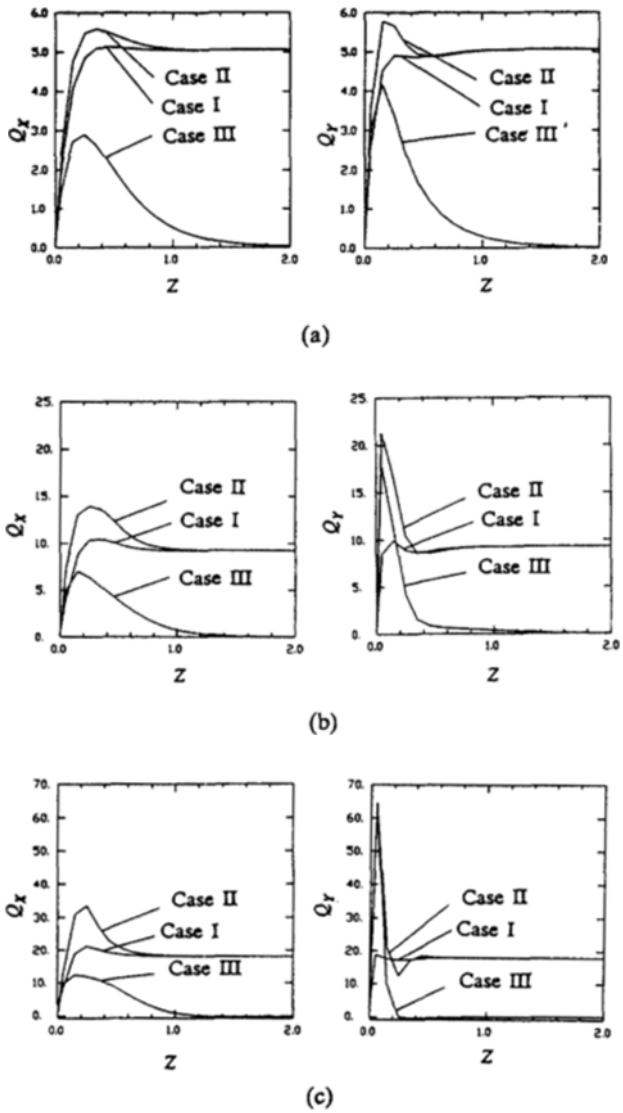

Fig. 9 Distributions of Q_X and Q_Y in the Z direction for $A_Z=4$, (a) $Ra=10^4$, (b) $Ra=10^5$, (c) $Ra=10^6$

4. CONCLUSION

In this study, Leonard's QUICK scheme is reformulated to obtain stable solutions for the three-dimensional natural convective flow. Several important observations are noted and summarized blow.

(1) A rotational flow induced by a temperature disturbance at the end wall reinforces the axial flow.

(2) A temperature disturbance imposed on the end walls magnifies the three dimensional effect.

(3) For the high Rayleigh numbers, three dimensionality of U velocity is stronger than that of V velocity.

ACKNOWLEDGEMENTS

The authors are grateful for the support provided by a grant from the Engineering Education and Research Foundation, College of Engineering, Seoul National University.

REFERENCES

Mallinson, G.D. and de Vahl Davis, G., 1977, "Three Dimensional Natural Convection in a Box : a Numerical study", *J. Fluid Mechanics*, Vol. 83, pp. 1~31.

Morrison, G.L. and Tran, V.Q., 1977, "Lamminar Flow Structure in Vertical Free Convective Cavities", *Int. J. Heat Mass Transfer*, Vol. 21, pp. 203~213.

Mallinson, G.D., 1987, "The Effects of Side Wall Conduction on Natural Convection in a Slot", *Journal of Heat Transfer*, Vol. 109, pp. 419~426.

Patankar, S.V., 1980, *Numerical Heat Transfer and Fluid Flow*, McGraw-Hill, New York.

Leonard, B.P., 1979, "A Stable and Accurate Convective Modelling Procedure Based on Quadratic Upstream Interpolation", *Computer Methods in Applied Mechanics and Engineering*, Vol. 19, pp. 59~98.